CREATIVE SCIENCE

Journal home page: csj.snru.ac.th

AI-driven multi-response optimization of perforated Ti-6Al-4V sheets via two-point incremental forming using an ANN–GA-based approach

Apisit Keawchaloon [a],Suriya Prasomthong [a], Thanatep Phatungthane [b] and Chaiya Chomchalao [a*]

[a] *Department of Industrial Technology, Nakhon Phanom University, Nakhon Phanom, 48000, Thailand*
[b] *Division of Science, Faculty of Education, Nakhon Phanom University, Nakhon Phanom, 48000, Thailand*

Abstract

Article history:

Received: 24-01-2026
Revised : 17-02-2026
Accepted: 19-02-2026
Published: 19-02-2026

Keywords:

Ti-6Al-4V; TPIF;
Taguchi-ANN-GA

This study investigates two-point incremental forming (TPIF) of perforated Ti-6Al-4V sheets using an integrated experimental–computational framework to optimize surface hardness and formability. Room-temperature TPIF of mill-annealed Grade 5 Ti-6Al-4V sheets (100 × 100 × 1 mm) was performed under dry conditions. Sheets with 2 mm holes at pitches of 6, 8, and 10 mm were formed following a Taguchi L9 design. Holes were produced by precision CNC drilling, ensuring clean edges without a heat-affected zone and preserving the base microstructure. Hole pitch (Hp), incremental step depth (ISD), and feed rate (Fr) were evaluated using Vickers hardness (HV) and forming depth (FD). Hole pitch was the dominant factor, contributing 59.1% to hardness and 69.2% to forming depth. An ANN (3–5–2) accurately predicted both responses (RMSE = 1.37 for HV; 0.0458 for FD) and was coupled with GA for multi-response optimization. The ANN–GA converged within 1000 generations and identified the optimum (Hp = 10 mm, ISD = 0.4 mm, Fr = 0.75 mm·min^{-1} , yielding HV and FD values of 341 and 9.92 mm, respectively. Validation experiments at the optimal condition showed <2% deviation from predictions. Improved performance was attributed to strain redistribution and localized work hardening around perforations. The novelty of this work lies in integrating perforation-assisted deformation mechanics with AI-driven multi-response optimization for a difficult-to-form titanium alloy. This approach offers a practical pathway for lightweight, high-strength titanium component design in aerospace, biomedical, and EV applications.

*** Corresponding author** : chaiwelding@ms.npu.ac.th

DOI: https://doi.org/10.55674/cs.v18i2.265879

1. Introduction

Titanium alloy Ti-6Al-4V (Grade 5) is widely used in aerospace, biomedical, and energy applications due to its high strength-to-weight ratio, corrosion resistance, and biocompatibility [1]. However, its room-temperature formability is limited by the dual-phase α+β microstructure, where the hexagonal close-packed (HCP) α-phase provides restricted slip systems and the β-fraction cannot sustain large uniform deformation [2]. Deformation is governed by planar slip and strain localization, with work hardening influenced by grain size and phase distribution, and strong temperature sensitivity due to the β-transus (~995 °C), below which ductility is constrained. These characteristics often lead to cracking, thinning, and dimensional inaccuracies in conventional forming.

Incremental sheet forming (ISF) offers a flexible die-less alternative, yet Ti-6Al-4V in single point incremental forming (SPIF) still exhibits high forming forces and thickness nonuniformity [3]. Two point incremental forming (TPIF) improves dimensional accuracy and reduces residual stress, with process parameters strongly affecting forming depth and hardness [4, 5]. Nevertheless, most studies focus on parameter optimization for solid sheets, while the effect of structural modification on strain redistribution remains underexplored. Introducing controlled perforations reduces the effective stiffness and alters stress-transfer paths, enabling localized strain accommodation near hole edges and progressive strain redistribution governed by ligament efficiency.

To address this gap, the current study investigates perforated Ti-6Al-4V sheets (planar dimensions 100 × 100 mm, thickness 1 mm) with 2 mm holes at pitches of 6–10 mm under TPIF. The hole size balances structural integrity and strain relief, while the pitch range corresponds to ligament efficiency ratios of 2–4. Process parameters were designed using Taguchi L9, while hardness (HV) and

forming depth (FD) were modeled by ANN and optimized via GA. Although 27 combinations exist, L9 minimizes the number of experiments, and ANN captures nonlinear interactions. The Taguchi–ANN–GA framework [6 – 9] links perforation-assisted deformation mechanics with AI-based multi-response optimization. Unlike conventional ANN–GA parameter tuning, the innovation lies in coupling structural sheet modification with intelligent modeling. The outcomes are relevant to thin-walled aerospace brackets, patient-specific biomedical plates, and lightweight EV structural panels requiring enhanced local formability and surface integrity.

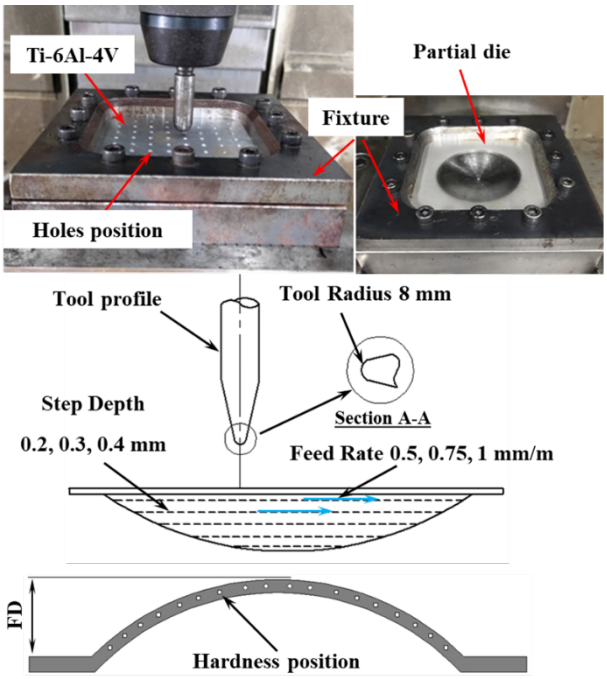

Fig. 1 TPIF setup, tool geometry, and measurement locations for perforated Ti-6Al-4V sheets.

2. Materials and Methods

Material

Grade 5 titanium alloy (Ti-6Al-4V) sheets (1 mm thick) were used. The supplier-certified composition was a Ti balance with 6.2 wt.% Al and 4.0 wt.% V plus minor Fe, O, C, and N [10]. Al stabilizes the α-phase (strength/oxidation resistance), while V stabilizes the β-phase (toughness/ductility at elevated temperature) [10]. The as-received sheets showed UTS ≈950 MPa, YS ≈880 MPa, elongation 14–16%, and hardness ≈340 HV [11]. Room-temperature formability is limited by the HCP α-phase and restricted slip, leading to strain localization, springback, thinning, and early fracture in conventional forming [12, 13]. Hence, incremental sheet forming—particularly TPIF—was adopted for localized deformation and improved dimensional accuracy [14, 15]. Figure 1 shows the setup, partial die, toolpath, and locations for hardness measurements.

$$S/N_{LTB} = -10\log_{10}\left(\frac{1}{n}\sum_{i=1}^{n}\frac{1}{y_i^2}\right). \quad (1)$$

Table 1 Process parameters and factor levels for ISF.

Parameter (Symbol)	-1	0	+1	Unit
Hole pitch (Hp)	6	8	10	mm
Incremental step depth (ISD)	0.2	0.3	0.4	mm
Feed rate (Fr)	0.5	0.75	1	mm·min^{-1}

Incremental setup and formability measurements

Figure 1 shows the perforated sheet, clamping system, and partial die used for TPIF. Forming was performed on a Cyclone VMC Series 610 CNC at the Faculty of Industrial Technology, Nakhon Phanom University [16], using a hemispherical tool with toolpaths generated in SolidWorks CAM based on a Taguchi L9 design [17]. Key parameters were ISD (0.2–0.4 mm) and feed rate (0.5–1.0 mm/min), with trajectories ensuring smooth transitions and uniform strain over the perforated area. Forming depth was measured at the pole using a digital height gauge (average of three readings). Samples were epoxy mounted, ground, polished, and evaluated by micro-Vickers indentation at designated locations for hardness testing [18].

Table 2 Taguchi L9 orthogonal array for ISF.

Run	Hp (mm)	ISD (mm)	Fr (mm·min^{-1})
1	6	0.2	0.5
2	6	0.3	0.75
3	6	0.4	1
4	8	0.2	0.75
5	8	0.3	1
6	8	0.4	0.5
7	10	0.2	1
8	10	0.3	0.5
9	10	0.4	0.75

Prediction and optimization

Taguchi experimental design The Taguchi method assessed the effects of Hp, ISD, and Fr on hardness (HV) and forming depth (FD) in TPIF of perforated Ti-6Al-4V sheets. Parameter levels and the L9 array are given in Tables 1–2. A larger-the-better S/N ratio was applied [19] and computed via Eq. (1) from repeated tests [8]. Normalized S/N ratios identified optimal settings, while main effects and ANOVA determined factor significance and dominant parameters for multi-response performance [19, 20].

ANN prediction modeling An ANN was built to predict hardness and forming depth in TPIF of perforated Ti-6Al-

4V using HP, ISD, and feed rate as inputs. A feed-forward 3–5–2 network (Fig. 2) was trained with the Levenberg–Marquardt algorithm for rapid, stable convergence. Learning rate and momentum were 0.5 and 0.4; transfer coefficients were 0.6 (input), 1.4 (hidden), and 0.6 (output), with a bias of 0.0005 to enhance generalization. Inputs were normalized via min–max scaling (Eq. 2) [7,9].

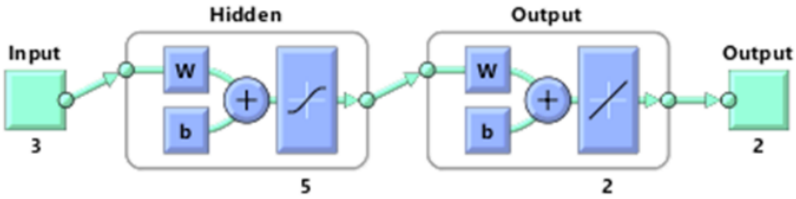

Fig. 2 ANN architecture illustrating data flow from the input to output layers.

$$X_i' = \frac{X_i - X_{i,min}}{X_{i,max} - X_{i,min}} \quad (2)$$

The transformation from the normalized input vector X′ to the predicted output vector Y′ is described by the hidden- and output-layer computations in Equations (3) and (4):

$$h = f(W^{(1)}X' + b^{(1)}) \quad (3)$$

$$Y' = f(W^{(2)}h + b^{(2)}) \quad (4)$$

where N is the number of experimental samples, $W^{(1)}$ and $W^{(2)}$ are the weight matrices, $b^{(1)}$ and $b^{(2)}$ are the bias vectors, and $f(\cdot)$ denotes the activation function. The trained ANN therefore establishes a robust nonlinear mapping between TPIF process parameters and the corresponding mechanical responses, providing an efficient surrogate model for subsequent optimization.

ANN–GA optimization The trained ANN was coupled with a genetic algorithm (GA) to optimize TPIF parameters for maximum hardness (HV) and forming depth (FD). The ANN functioned as a surrogate for fast fitness evaluation. The multi-objective task was converted to a weighted single fitness function (Eq. 5) with $\omega_1 + \omega_2 = 1$, and constraints were enforced via a penalty function (Eq. 6) within bounds (L_i, U_i). This ANN–GA integration enabled efficient global search and identification of optimal forming conditions with improved performance [7, 9].

$$\text{Fitness} = \omega_1\left(\frac{HV}{HV_{max}}\right) + \omega_2\left(\frac{FD}{FD_{max}}\right) \quad (5)$$

$$P(x) = \rho\sum_{i=1}^{n}[max(0, x_i - U_i)^2 + max(0, L_i - x_i)^2], \quad (6)$$

Validation of the ANN–GA model The ANN–GA model was validated using R^2, RMSE, and MAPE. Data were split into training (70%), validation (20%), and testing (10%) sets. R^2 quantified agreement between predicted and experimental hardness or forming depth (Eq. 7), while RMSE and MAPE measured absolute and relative errors (Equations 8–9), with N as sample size. High R^2 and low RMSE/MAPE indicate strong accuracy and generalization for multi-response prediction and optimization.

$$R^2 = 1 - \frac{(\sum_{i=1}^{n}(Y_i^{(exp)} - Y_i^{(pred)})^2}{(\sum_{i=1}^{n}(Y_i^{(exp)} - \bar{Y}^{(pred)})^2} \quad (7)$$

$$RMSE = \sqrt{\frac{1}{N}\sum_{i=1}^{N}(Y_i^{(exp)} - Y_i^{(pred)})^2} \quad (8)$$

$$MAPE = \frac{100}{N}\sum_{i=1}^{N}\left|\frac{(Y_i^{(exp)} - Y_i^{(pred)})}{Y_i^{(exp)}}\right|, \quad (9)$$

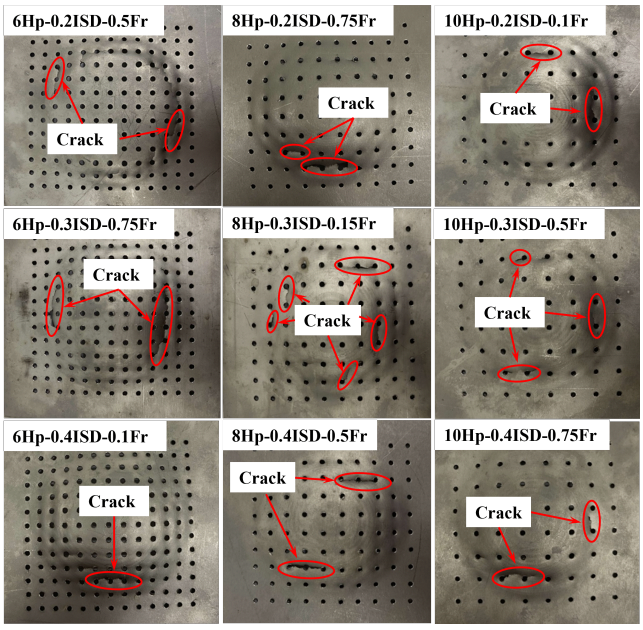

Fig. 3 Crack and failure modes of perforated Ti-6Al-4V sheets after TPIF under varying parameters.

3. Results and Discussion

Surface morphology of formed specimens

Figure 3 shows the crack morphology of perforated Ti-6Al-4V sheets formed under various TPIF conditions, emphasizing the roles of Hp, ISD, and Fr. A smaller Hp (6 mm) resulted in fewer and shallower cracks due to more uniform load distribution and better strain accommodation. Larger pitches (8–10 mm) caused stress concentrations at hole edges, promoting multiple crack initiation sites and propagation along shear zones. Higher ISD increased plastic strain per pass, producing deeper cracks and local thinning near the forming pole. Likewise, high feed rates limited material flow by reducing dwell time, leading to premature fracture. Overall, a small hole pitch, moderate ISD, and low Fr effectively reduce cracking and improve deformation stability during TPIF of perforated Ti-6Al-4V sheets.

Taguchi analysis

The Taguchi method was used to evaluate the effects of Hp, ISD, and Fr on HV and FD during TPIF of perforated Ti-6Al-4V sheets. Experimental outcomes and corresponding signal-to-noise (S/N) ratios are listed in Table 3. As both responses indicate improved mechanical performance and formability, the larger-the-better criterion was applied.

To enhance interpretation, the safe process window was identified between Hp = 6–8 mm and ISD ≤ 0.3 mm, where stable deformation occurred without catastrophic cracking. This range defines the operational forming window for perforated Ti-6Al-4V under the studied TPIF conditions.

Table 3 TPIF results and S/N ratios.

Run	Hp	ISD	Fr	HV	FD	SN/ HV	SN/ FD
1	6	0.2	0.5	315.4	7.75	49.98	17.79
2	6	0.3	0.75	329.6	7.95	50.36	18.01
3	6	0.4	1	318.7	9.32	50.07	19.39
4	8	0.2	0.75	334.9	8.45	50.50	18.54
5	8	0.3	1	336.1	8.65	50.53	18.74
6	8	0.4	0.5	338.8	8.6	50.60	18.69
7	10	0.2	1	323.6	9.83	50.20	19.85
8	10	0.3	0.5	335.5	9.65	50.51	19.69
9	10	0.4	0.75	340.8	9.95	50.65	19.96

ANOVA was used to quantified parameter significance. For HV (Table 4), Hp was dominant (59.10%), followed by ISD (22.50%) and Fr (18.20%). The regression model showed excellent agreement with the data (R^2 = 99.71%, R^2(adj) = 98.85%) and minimal residual error (0.20%). These results suggest that smaller Hp enhances stress transfer and localized strain hardening in the perforated structure, improving surface hardness.

Table 4 ANOVA of HV S/N ratios for TPIF.

Source	DF	Seq SS	Adj SS	Adj MS	F-value	P-value	% Con.
Hp	2	0.276	0.276	0.138	204.45	0.005	59.10
ISD	2	0.105	0.105	0.053	77.99	0.013	22.50
Fr	2	0.085	0.085	0.043	63.07	0.016	18.20
Res.E	2	0.001	0.001	0.001	0.000	0.000	0.20
Total	8	0.467	0.000	0.000	0.000	0.000	100.00

S = 0.0260; R-Sq = 99.71%; R-Sq(adj) = 98.85%

For FD (Table 5), Hp was the dominant factor (69.20%), followed by ISD (13.30%) and Fr (12.20%). The high determination coefficient (R^2 = 94.70%) indicates good model adequacy, while the residual contribution (5.30%) reflects geometric variability inherent to TPIF. Larger forming depths occurred at moderate step depths (0.3–0.4 mm) and higher feed rates (0.75–1.0 mm·min^{-1}), promoting stable plastic flow without premature fracture.

Table 5 ANOVA of FD S/N ratios for TPIF.

Source	DF	Seq SS	Adj SS	Adj MS	F-value	P-value	% Con.
Hp	2	3.524	3.524	1.762	13.06	0.071	69.20
ISD	2	0.676	0.676	0.338	2.50	0.285	13.30
Fr)	2	0.621	0.621	0.310	2.30	0.303	12.20
Res. E	2	0.270	0.270	0.135	0.000	0.000	5.30
Total	8	5.090	0.000	0.000	0.000	0.000	100.00

S = 0.3673; R-Sq = 94.70%; R-Sq(adj) = 78.80%

Overall, Taguchi analysis identifies Hp as the primary parameter controlling both hardness and formability via stress redistribution around perforations, while step depth and Fr provide secondary control over strain accumulation. These results support subsequent multi-response optimization using the ANN–GA framework to determine optimal TPIF parameters.

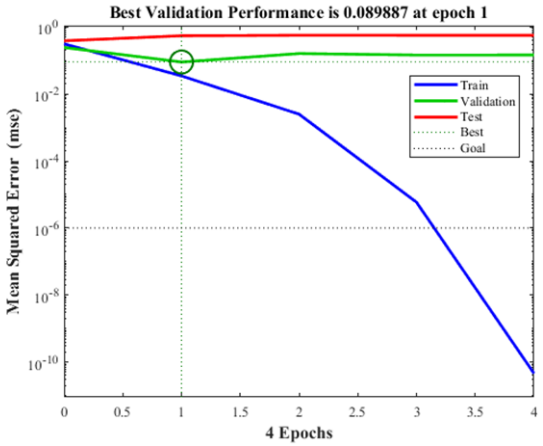

Fig. 4 MSE convergence during ANN training.

Modeling and Optimization

Figure 4 presents ANN training performance, showing mean squared error (MSE) trends for training, validation, and testing. The best validation result (MSE = 0.089887) occurred at epoch 1. The decreasing training MSE confirms effective learning of the nonlinear links between TPIF parameters and responses (hardness and forming depth). The close alignment of all curves indicates strong generalization with minimal overfitting, demonstrating high predictive reliability of the ANN model for TPIF of perforated Ti-6Al-4V sheets.

Table 6 compares experimental HV with ANN, Taguchi, and linear regression predictions for TPIF of perforated Ti-6Al-4V sheets. ANN showed the best accuracy (RMSE =

1.37, MAE = 1.05, MAPE = 0.32%), effectively capturing the nonlinear effects of hole pitch, ISD, and feed rate. Taguchi had larger errors (RMSE = 5.02, MAE = 3.91, MAPE = 1.17%), while linear regression performed close to ANN (RMSE = 1.45, MAE = 1.08, MAPE = 0.34%), but was less effective for complex interactions. Overall, ANN offers the most reliable hardness prediction for TPIF optimization.

Table 6 Experimental vs. predicted HV (ANN, Taguchi, LR) in TPIF.

Run	Exp.	ANN model	Taguchi model	Regression model
1	315.4	316.2	323.1	317.1
2	329.6	330.3	329.7	329.1
3	318.7	319.8	322.3	319.5
4	334.9	334.5	336.0	334.8
5	336.1	336.5	336.4	336.0
6	338.8	338.0	335.9	337.2
7	323.6	324.9	331.3	324.9
8	335.5	335.1	333.2	335.7
9	340.8	341.0	336.1	341.3
RMSE		1.37	5.02	1.45
MAE		1.05	3.91	1.08
%MAPE		0.32	1.17	0.34

Table 7 Experimental vs. predicted FD (ANN, Taguchi, LR) in TPIF.

Run	Exp.	ANN model	Taguchi model	Regression model
1	7.75	7.80	8.09	7.86
2	7.95	8.03	8.27	8.00
3	9.32	9.38	9.02	9.12
4	8.45	8.44	8.61	8.54
5	8.65	8.70	8.85	8.69
6	8.60	8.55	8.80	8.66
7	9.83	9.91	9.38	9.73
8	9.65	9.58	9.43	9.70
9	9.95	9.92	9.68	9.88
RMSE		0.0458	0.27	0.07
MAE		0.0349	0.22	0.05
%MAPE		0.4200	2.46	0.52

Table 7 compares experimental and predicted FD from ANN, Taguchi, and linear regression models. ANN achieved the highest accuracy with the lowest errors (RMSE = 0.0458, MAE = 0.0349, MAPE = 0.42%), effectively capturing nonlinear process–response behavior. The Taguchi model showed larger errors, while linear regression provided moderate accuracy but lower precision for complex interactions. Overall, ANN showed the closest agreement with experiments, confirming its suitability for FD prediction and TPIF optimization.

Figures 5(a,b) compare ANN, Taguchi, and regression predictions with experimental hardness and forming depth. ANN and regression closely match the data, capturing nonlinear process–response behavior, whereas Taguchi shows larger deviations due to linear averaging. Overall, ANN delivers the highest accuracy, confirming its robustness for modeling TPIF of perforated Ti-6Al-4V sheets.

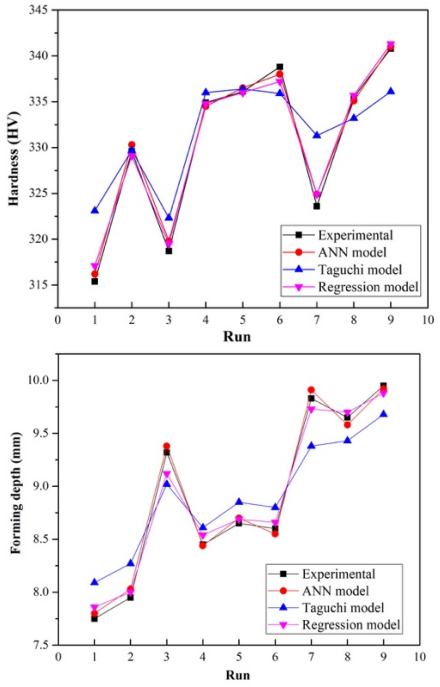

Fig. 5 Experimental vs. predicted ANN, Taguchi, and regression results for (a) hardness, and (b) forming depth in TPIF.

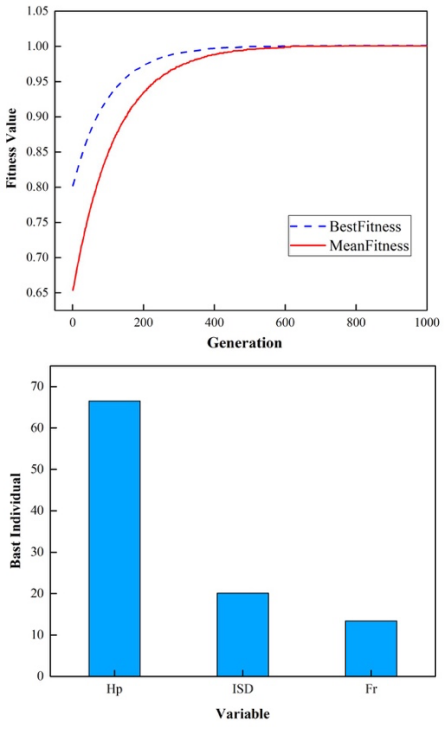

Fig. 6 ANN–GA optimization: (a) best/mean fitness convergence, and (b) parameter contribution to the optimum.

ANN–GA Optimization

Figure 6 shows ANN–GA convergence and parameter influence. In Fig. 6(a), best and mean fitness rise rapidly in the first 200 generations and stabilize after ~600, with a small gap at 800 generations indicating near-global convergence. Figure 6(b) identifies Hp as dominant (~67%), followed by ISD (~20%) and Fr (~13%), emphasizing the key role of perforation spacing in strain localization, plastic flow, and the resulting hardness and forming depth during TPIF of Ti-6Al-4V sheets.

Table 8 summarizes the optimal TPIF parameters identified by the ANN–GA framework. The global optimum was achieved at a Hp of 10 mm, ISD of 0.4 mm, and Fr of 0.75 mm·min^{-1}, resulting in a predicted hardness of 341 HV and forming depth of 9.92 mm with a desirability index of 1.000. These results confirm that the ANN–GA model effectively captures nonlinear parameter interactions and enables simultaneous optimization of hardness and formability in perforated Ti-6Al-4V sheets.

Table 8 Optimal ANN–GA TPIF parameters for perforated Ti-6Al-4V

Parameter	Optimal Value	Unit	Optimization Objective
Hp	10	mm	–
ISD	0.4	mm	–
Fr	0.75	mm·min^{-1}	–
Pre. HV	341	HV	Maximize
Pre. FD	9.92	mm	Maximize
D	1	–	Multi-response optimum

Discussion

The ANN–GA framework showed strong capability in modeling and optimizing nonlinear interactions between TPIF parameters and mechanical responses of perforated Ti-6Al-4V sheets [21]. The close match between experimental and predicted results—high R^2 with low RMSE and MAPE—confirms accurate representation of coupled effects from hole pitch, ISD, and Fr [22]. The Levenberg–Marquardt–trained ANN ensured rapid, stable convergence, reliably capturing nonlinear deformation behavior governing hardness and forming depth [23]. GA integration enabled efficient global search, converging toward parameters that simultaneously maximized hardness and formability [24].

From a materials viewpoint, the optimized parameters align with Ti-6Al-4V deformation mechanisms. Larger Hp promotes strain localization and plastic flow, while moderate ISD and Fr limit stress concentration, delaying crack initiation and improving strain uniformity. Hardness enhancement is linked to localized work hardening and partial dynamic recovery in the α+β microstructure under cyclic strain [12]. Perforation thus reduces effective stiffness while enhancing local ductility and overall formability.

Overall, hybrid AI optimization outperforms conventional Taguchi or RSM approaches in nonlinear, multi-response manufacturing problems [21, 24, 25]. The ANN–GA framework delivers high accuracy and efficiency, reducing experimental cost and time while providing a robust data-driven basis for intelligent optimization of titanium incremental forming processes.

4. Conclusions

This study developed an ANN–GA framework for optimizing TPIF parameters of perforated Ti-6Al-4V sheets. The ANN accurately captured nonlinear interactions among hole pitch, ISD, and feed rate, and GA optimization identified the optimum (Hp = 10 mm, ISD = 0.4 mm, Fr = 0.75 mm·min^{-1}), achieving a 341 HV hardness and a 9.92 mm forming depth.

Prediction errors were reduced to RMSE = 1.37 HV and 0.0458 mm, outperforming Taguchi and regression models. Performance improvement is attributed to strain redistribution and localized work hardening in the α+β microstructure. The key contribution is coupling structural perforation with AI-based multi-response optimization, rather than parameter tuning alone. Compared with conventional Taguchi methods, the approach reduces the number of experiments (L9 vs. 27) and better represents nonlinear behavior.

The study is limited to experimental–AI analysis of 1 mm sheets without FEM validation. Future work will extend the framework to other thicknesses and numerical modeling. Practically, the findings guide the manufacture of thin-walled aerospace, biomedical, and EV components requiring enhanced local formability. The framework supports data-driven intelligent forming aligned with Industry 4.0.

5. Suggestions

Future work should integrate real-time process monitoring and adaptive control with the ANN–GA framework to enable closed-loop optimization for smart TPIF systems. Incorporating additional process variables and in-situ data streams would further enhance model robustness and support Industry 4.0–oriented, data-driven manufacturing of advanced titanium alloys.

6. Acknowledgements

The authors gratefully acknowledge the Department of Machine Tool Technology, Faculty of Industrial Technology, Nakhon Phanom University, for providing research facilities, equipment, and machining resources essential to this study. The authors also sincerely thank Mrs. Nittaya Kaewchalun for her constant encouragement and financial support throughout the research work.

7. Declaration of Generative AI in Scientific Writing

The authors declare that generative artificial intelligence (AI) tools were used solely to assist in improving the language clarity, grammar, and academic style of the

manuscript. The scientific content, experimental design, data analysis, interpretation of results, and conclusions were entirely conceived and validated by the authors. All responsibility for the accuracy, originality, and integrity of the work rests with the authors.

8. CRediT Author Statement

Apisit Keawchalun: Conceptualization, Methodology, Investigation, Data Curation, Writing – Original Draft.

Suriya Prasomthong: Methodology, Formal Analysis, Writing – Review & Editing.

Thanatep Phatungthane: Formal Analysis, Validation.

Chaiya Chomchalao: Conceptualization, Supervision, Project Administration.

9. Research Involving Human and Animals Rights

This study did not involve any experiments on human participants or animals. Therefore, ethical approval and informed consent were not required.

10. Ethics Approval and Consent to Participate

Not applicable. This study did not involve human participants or animals, and therefore ethics approval and informed consent were not required.

11. Declaration of Competing Interest

The authors declare that they have no known competing financial interests or personal relationships that could have appeared to influence the work reported in this paper.

12. References

[1] Rabbitt, D., Villapún, V. M., Carter, L. N., Man, K., Lowther, M., O'Kelly, P., & Cox, S. C. (2025). Rethinking biomedical titanium alloy design: A review of challenges from biological and manufacturing perspectives. *Advanced Healthcare Materials, 14*(4), 2403129. https://doi.org/10.1002/adhm.202403129

[2] Badr, O. M., Barlat, F., Rolfe, B., Lee, M. G., Hodgson, P., & Weiss, M. (2016). Constitutive modelling of high strength titanium alloy Ti-6Al-4V for sheet forming applications at room temperature. *International Journal of Solids and Structures, 80*, 334–347. https://doi.org/10.1016/j.ijsolstr.2015.08.025

[3] Oleksik, V., Trzepieciński, T., Szpunar, M., Chodoła, Ł., Ficek, D., & Szczęsny, I. (2021). Single-point incremental forming of titanium and titanium alloy sheets. *Materials, 14*(21), 6372. https://doi.org/10.3390/ma14216372

[4] Morita, T., Oka, Y., Tsutsumi, S., Takesue, S., Higuchi, N., & Sakai, H. (2022). Short-time heat treatment for Ti-6Al-4V alloy produced by selective laser melting. *Materials Transactions, 63*(6), 854–863. https://doi.org/10.2320/matertrans.MT-M2022018

[5] Charonerat, S., Onbut, K., Prasomthong, S., Pookamnerd, Y., & Thosa, P. (2025). Multi-objective optimization of two-point incremental forming parameters for Ti-6Al-4V using Taguchi approach. *EUREKA: Physics and Engineering*, (5), 132–143. https://doi.org/10.21303/2461-4262.2025.003904

[6] Prasomthong, S., & Onbat, K. (2023). The optimization of sheet forming on residual stress and surface roughness with two-point incremental forming process (TPIF) of aluminum alloy parts. *Applied Science and Engineering Progress, 16*(4), 6059. https://doi.org/10.14416/j.asep.2022.06.003

[7] Prasomthong, S., Phatungthane, T., & Chomchalao, C. (2025). Optimization of aluminum matrix composite production in a friction stir process with MgO nanoparticle reinforcement using ANN–GRA modeling. *Engineering and Applied Science Research, 52*(3), 282–295. https://ph01.tci-thaijo.org/index.php/easr/article/view/259404

[8] Pookamnerd, Y., Thosa, P., Charonerat, S., & Prasomthong, S. (2023). Development of mechanical property prediction model and optimization for dissimilar aluminum alloy joints with the friction stir welding (FSW) process. *EUREKA: Physics and Engineering*, (3), 112–128. https://doi.org/10.21303/2461-4262.2023.002776

[9] Mayai, A., Prasomthong, S., & Pookamnerd, Y. (2025). Development of hybrid ANN–GA and RSM models for optimizing mechanical properties in SS400–SUS304 welds. *EUREKA: Physics and Engineering*, (3), 152–165. https://doi.org/10.21303/2461-4262.2025.003606

[10] Tandecka, K., Kacalak, W., Wieczorowski, M., & Mathia, T. G. (2024). Evaluation of Surface Finishing Efficiency of Titanium Alloy Grade 5 (Ti–6Al–4V) After Superfinishing Using Abrasive Films. *Materials*, *17*(21), 5198. https://doi.org/10.3390/ma17215198.

[11] Badr, O. M. (2015). Forming of high strength titanium sheet at room temperature. *Materials & Design, 66*, 428–437. https://doi.org/10.1016/j.matdes.2014.03.008

[12] Ao, D. (2020). Formability and deformation mechanism of Ti–6Al–4V sheet by incremental forming. *Journal of Materials Processing Technology, 282*, 116703. https://doi.org/10.1016/j.jmatprotec.2020.116703

[13] Trzepieciński, T., Szpunar, M., Ostrowski, R., Ziaja, W., & Motyka, M. (2024). Advanced FEM insights into pressure-assisted warm single-point incremental forming of Ti–6Al–4V titanium alloy sheet metal. *Materials, 14*(6), 619. https://doi.org/10.3390/met14060619

[14] Bansal, A., Jiang, B., & Ni, J. (2019). Die-less fabrication of miniaturized parts through single point incremental micro-forming. *Journal of Manufacturing Processes, 43*, 20–25. https://doi.org/10.1016/j.jmapro.2019.03.046

[15] Emmens, W. C., Sebastiani, G., & van den Boogaard, A. H. (2010). The technology of incremental sheet forming—A brief review of the history. *Journal of Materials Processing Technology, 210*(8), 981–997. https://doi.org/10.1016/j.jmatprotec.2010.02.014

[16] Ou, L., An, Z., Gao, Z., Zhou, S., & Men, Z. (2020). Effects of Process Parameters on the Thickness Uniformity in Two-Point Incremental Forming (TPIF) with a Positive Die for an Irregular Stepped Part. *Materials*, *13*(11), 2634. https://doi.org/10.3390/ma13112634.

[17] Moharam, L. M., El-Hoshy, A. Z., & Abou-Elenein, K. (2017). The effect of different insertion techniques on the depth of cure and vickers surface micro-hardness of two bulk-fill resin composite materials. *Journal of Clinical and Experimental Dentistry*, *9* (2), e266 - e271. https://doi.org/10.4317/jced.53356.

[18] Wu, H., Dave, F., Mokhtari, M., Ali, M. M., Sherlock, R., Mcilhagger, A., Tormey, D., & McFadden, S. (2022). On the Application of Vickers Micro Hardness Testing to Isotactic Polypropylene. *Polymers*, *14*(9), 1804. https://doi.org/10.3390/polym14091804.

[19] Charonerat, S., Onbut, K., Prasomthong, S., Pookamnerd, Y., & Thosa, P. (2025). Multi-objective optimization of two-point incremental forming parameters for Ti-6Al-4V using

taguchi approach. *EUREKA: Physics and Engineering*, (5), 132-143. https://doi.org/10.21303/2461-4262.2025.003904.

[20] Tekade, R. K., & Chougule, M. B. (2013). Formulation development and evaluation of hybrid nanocarrier for cancer therapy: Taguchi orthogonal array based design. *BioMed Research International, 2013*, 712678. https://doi.org/10.1155/2013/712678

[21] Hisam, M. W., Dar, A. A., Elrasheed, M. O., Khan, M. S., Gera, R., & Azad, I. (2024). The versatility of the Taguchi method: Optimizing experiments across diverse disciplines. *Journal of Statistical Theory and Applications, 23*(4), 365–389. https://doi.org/10.1007/s44199-024-00093-9

[22] Xiao, X., Zhang, X., Zhang, Y., & Tang, J. (2020). RSM and BPNN modeling in incremental sheet forming process for AA5052 sheet: Multi-objective optimization using genetic algorithm. *Metals, 10*(8), 1003. https://doi.org/10.3390/met10081003

[23] Equbal, A., Khan, M. S., Shandilya, S., & Alam, N. (2020). Application of the combined ANN and GA for multi-response optimization of cutting parameters for the turning of glass fiber-reinforced polymer composites. *Mathematics, 8*(6), 947. https://doi.org/10.3390/math8060947

[24] Maurya, A. K., Verma, A. K., Singh, P. S., & Singh, N. (2025). Artificial neural network modeling of Ti-6Al-4V alloys to correlate their microstructure and mechanical properties. *Materials, 18*(5), 1099. https://doi.org/10.3390/ma18051099

[25] Sahib, M. M., & Kovács, G. (2024). Multi-objective optimization of composite sandwich structures using artificial neural networks and genetic algorithm. *Results in Engineering, 21*, 101937. https://doi.org/10.1016/j.rineng.2024.101937